Optical In-Situ Assessment of a Nonimaging Secondary Concentrator in a Solar Tower

Abraham Kribus*
Mem. ASME
Environmental Sciences and
Energy Research Department,
Weizmann Institute of Science,
Rehovot 76100, Israel
e-mail: avi.kribus@weizmann.ac.il

Andreas Timinger
Optics & Energy Concepts,
Paul-Gerhardt-Allee 42,
D-81245 Munich, Germany

A method for remote optical measurement of the geometry of nonimaging concentrators is presented. A concentrator installed in a solar tower was measured by observation of transmission patterns from the heliostat field, and comparison of the measured patterns to a ray tracing simulation. The actual geometry of the concentrator was derived from optimization of the match between real and simulated patterns. The measurement was sensitive and accurate enough to detect small errors in the concentrator geometry, such as 1 millimeter in linear dimension and 0.1° in concentrator tilt angle. The measurement procedure is simple and can be easily adapted to a wide range of nonimaging optical systems. [DOI: 10.1115/1.1488668]

1 Introduction

Nonimaging reflective concentrators are used for concentration of solar radiation, especially as second stage concentrators for high-temperature solar power plants [1]. Secondary concentrators may be relatively small devices when the primary is a parabolic dish [2,3] or large devices intended for solar tower systems [4,5]. The use of secondary concentrators can increase the flux incident on the solar receiver relative to the use of only one concentrator stage, because the potential of a two-stage system may approach the thermodynamic limit of concentration [6]. Reaching a high incident flux is important in high-temperature applications, for example power generation with modern engines such as gas turbines [5,7] and solar chemistry [8,9,10]. A high incident flux provides high receiver efficiency in spite of the high temperature, and is therefore a crucial element in the overall process efficiency.

The performance of a nonimaging concentrator is sensitive to the geometric accuracy of its reflective surfaces. Generally, it is difficult to assess the optical performance of an existing nonimaging concentrator, or to measure its geometry with sufficient resolution and precision. This is especially difficult for large concentrators that are assembled *in-situ* from many separate elements, and their reflective surfaces are not easily accessible after assembly for a physical measurement. In these cases, it is possible to perform calorimetric measurements that determine the overall power exiting the concentrator [11,12], and flux measurements at the exit aperture [5]. These provide only limited detail, and offer no information on how the actual device geometry deviates from the design. If concentrator performance is much lower than anticipated due to manufacturing flaws, such measurements provide little assistance in identifying and repairing these flaws. A more detailed geometric characterization of imaging reflectors can be provided by photogrammetry [13], which was successfully used with a primary concentrator. This is not practical for a large nonimaging secondary, because it requires a direct line of sight to, and physical manipulation of, the internal reflective surfaces.

We have developed an all-optical remote measurement method for nonimaging concentrators and demonstrated its application in the laboratory measurement of a small concentrator [14]. In this contribution, we demonstrate the method *in-situ*, with a secondary concentrator installed on a solar tower and the measurements performed remotely from within the heliostat field. The concentrator chosen for this test was an asymmetric device with rectangular cross-section, which was optimized for accepting radiation from an East-West wide field [15]. The measurements included placing a Lambertian source across the concentrator's exit aperture, taking photographs of the concentrator from strategically selected points in the field, and analysis of the transmission patterns visible in the photographs. The final product of the analysis was a calibrated geometrical description of the concentrator, which can be used to predict performance under any conditions and to assess any needed repairs or adjustments of concentrator geometry.

2 Principles of Remote *In-Situ* Measurement. The remote measurement method was previously presented in detail [14], and a brief summary is provided here for completeness. The method is based on the reversibility of ray-paths in the framework of geometric optics, assuming surfaces that are specularly reflecting and non-emitting. A path through the concentrator represents both a ray starting at the entrance aperture, and another starting at the exit aperture. Hence, all rays that are accepted by a concentrator (enter through the inlet, and reach the exit aperture) can be reversed by placing a Lambertian source across the exit aperture, and observing what comes out of the inlet aperture. Looking onto the entrance aperture of the concentrator, a pattern is observed of bright regions illuminated by the radiation source and dark regions that are not illuminated. This corresponds to the transmission pattern [1] for radiation emerging from the position of observation. Radiation coming from the point of observation and falling on the illuminated regions of the inlet aperture will be accepted, because these paths lead to the exit aperture; rays coming from that position and falling on the dark regions will be rejected. An illustration of the receiver and typical rays passing through transmission and rejection regions of the aperture is presented in Fig. 1. A series of photographs from different positions of observation can provide values of the transmission function for a set of incident directions for each point on the entrance aperture.

It may be convenient to take the photographs directly from the position of the source of radiation that the concentrator is designed to accept, i.e., from the parabolic dish or the heliostat field that serve as primary concentrator. This choice will provide the transmission information directly in the relevant positions. However, the measurements may also be taken from another set of observation points without loss of information about the transmission function. This is since the measurements show the directional dependence of the transmission pattern, which is only weakly influenced by the distance from the observation point to the target.

Performing many observations from different directions relative

*Current address: Fluid Mechanics and Heat Transfer Department, Tel Aviv University, Tel Aviv 69978, Israel, e-mail: kribus@eng.tau.ac.il

Contributed by the Solar Energy Division of the THE AMERICAN SOCIETY OF MECHANICAL ENGINEERS for publication in the ASME JOURNAL OF SOLAR ENERGY ENGINEERING. Manuscript received by the ASME Solar Energy Division, November 2000; final revision, February 2002. Associate Editor: R. Hogan.

to the target, corresponding to different positions within a reference surface such as the primary concentrator, can provide a complete map of the transmission of radiation through the concentrator, with full four-dimensional (4-D) resolution within the phase space of geometric optics [14]. It is, therefore, possible to recover the geometry of the concentrator that creates this mapping in phase space. The other diagnostic methods mentioned above involve loss of information: calorimetry collapses all transmission information to a single integral value, and flux measurement reduces the information from four to two dimensions. This integration within the 4-D phase space results in a loss of information, which makes it impossible to recover the geometry of the actual concentrator from the results.

3 Experimental Method

The optical assessment method was applied to a secondary concentrator installed at the 9th floor of the solar tower at the Weizmann Institute of Science. The concentrator has a rectangular entrance aperture and a rectangular exit aperture. It is composed of eight plane facets of trapezoidal shape, as shown in Fig. 1. This geometry was optimized to accept radiation coming from the whole field of heliostats [15], and is not limited to an axisymmetric acceptance cone typical of more conventional designs. This concentrator can serve as part of an array of concentrators, following the partitioned receiver concept [16,17], due to its rectangular aperture. The geometrical concentration is 4.5, and the transmission efficiency is 92.7% assuming 95% reflectivity. The nominal flux concentration hence is 4.17. A more detailed description of the design, construction and calorimetric testing of the concentrator can be found in [11,15].

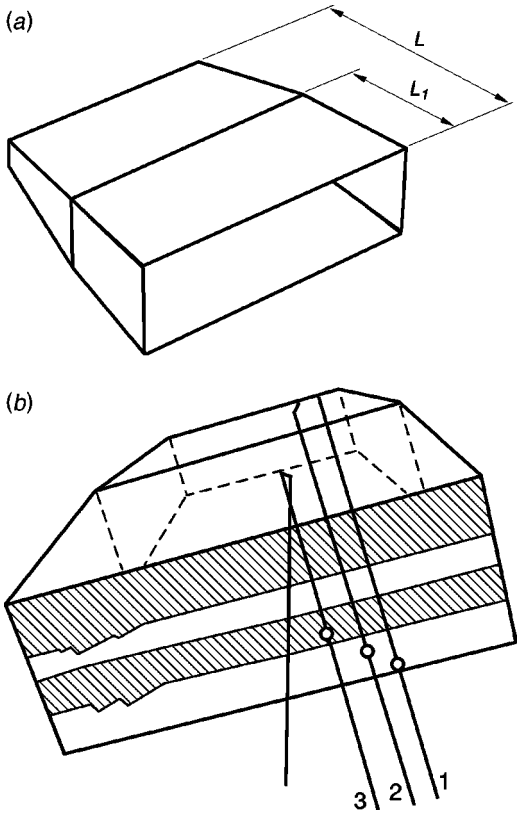

Fig. 1 (a) The geometry of the rectangular concentrator used for the remote *in-situ* measurement. Eight plane facets of trapezoidal shape interconnect a rectangular entrance aperture and a rectangular exit aperture. (b) Representative rays entering the aperture through a transmission region (white) and a rejection region (hatched); white circles indicate the points of penetration at the inlet aperture. Rays 1 and 2 reach the exit aperture directly and after one reflection, respectively. Ray 3 is rejected after two reflections.

In the laboratory measurement [14], we have used an active light source at the exit aperture, and the ambient light was suppressed. The patterns that were produced were therefore composed of easily distinguished bright and dark regions. In an *in-situ* measurement, it is more difficult to suppress ambient light. It may be possible to perform the measurement at night, if there is not too much artificial ambient light present. However, in a daytime measurement, the regions representing rejected rays in the transmission patterns are not dark. They contain reflected ambient light from the sky or from the heliostat field. It is, therefore, not possible to analyze the transmission patterns based on brightness, as was done in the laboratory test.

The contrast between transmission and rejection regions was produced in the current test using color. The Lambertian source was constructed by placing a flat piece of bright orange cardboard across the exit aperture of the concentrator. The rough cardboard reflected incident light diffusely, in all directions within the hemisphere facing the primary concentrator. This reflected light could be easily distinguished from ambient light by its color. The source was not exactly Lambertian, since the outgoing radiation was not necessarily at uniform intensity. The analysis of the transmission patterns, therefore, used a color criterion to distinguish between orange and non-orange regions, rather than a brightness criterion.

Photographs of the entrance aperture were taken from seven positions within the heliostat field. Figure 2 shows the layout of the WIS heliostat field and the observation positions. The equal transmission contour lines indicate the acceptance range of the concentrator, according to ray-tracing simulation. The relatively sharp transition from high to low transmission shows the good adaptation of the concentration optics to the eccentric shape of the heliostat field.

Observation positions 1–6 were selected within the transition region near the edge of the acceptance range, since the sensitivity of the transmission patterns to small geometric changes in the concentrator is highest in this region [14]. The patterns seen from within the transition region are composed of regions that are illuminated bright orange by the Lambertian source across the exit aperture, and regions that reflect ambient light and do not show the source color. The intensity in the bright orange regions was essentially uniform, except for small variations due to different number of reflections at the concentrator's walls that incur absorption losses.

Position 7 was chosen approximately at the center of the field, where transmission is close to 100%. The observation from this position showed the full entrance aperture filled with bright orange radiation from the source, with no significant ray rejection. For this reason, the measurement from position 7 requires no analysis, and provides no useful information other than to confirm the ray tracing result of complete transmission.

Images of the transmission patterns at each position were taken using a camera with ASA 100 color slide film. An appropriate lens was chosen such that the concentrator entrance aperture fills a significant part of the picture, to provide sufficient image resolution. The acquired image resolution exceeded the resolution of the simulated image (Section 4.2), and therefore was not a limiting factor on the accuracy of the analysis. In principle, image resolution can be affected by the lens quality and by distortion due to thermal gradients in the air intervening between the observation point and the target. We have found that the image quality was sufficient to resolve the small features that were predicted by the simulation, and that the images seemed stable and reproducible. The lens and atmosphere effects were therefore not significant in the current tests. Additional experience with larger solar plants and under various atmospheric conditions is needed to validate this conclusion.

4 Analysis of the Transmission Patterns

4.1 Image Processing. The pictures were scanned from the color slides for further processing. The scanning resolution was adjusted to provide about 45,000 pixels within the aperture, which matches the resolution of the simulated images (see Section 4.2). No processing or filtering was applied to the image during the scanning process. Figure 3 shows a typical scanned transmission pattern as photographed from position 1. The transmission regions can be identified as horizontal strips of nearly uniform gray, representing the bright orange of the original photographs. The regions that reflect ambient light show a variety of patterns, including images of heliostats that are much brighter than the radiation coming from the source. Nevertheless, the color criterion used to identify the transmission regions does not depend on relative brightness, and therefore, the ambient light does not affect the measurement.

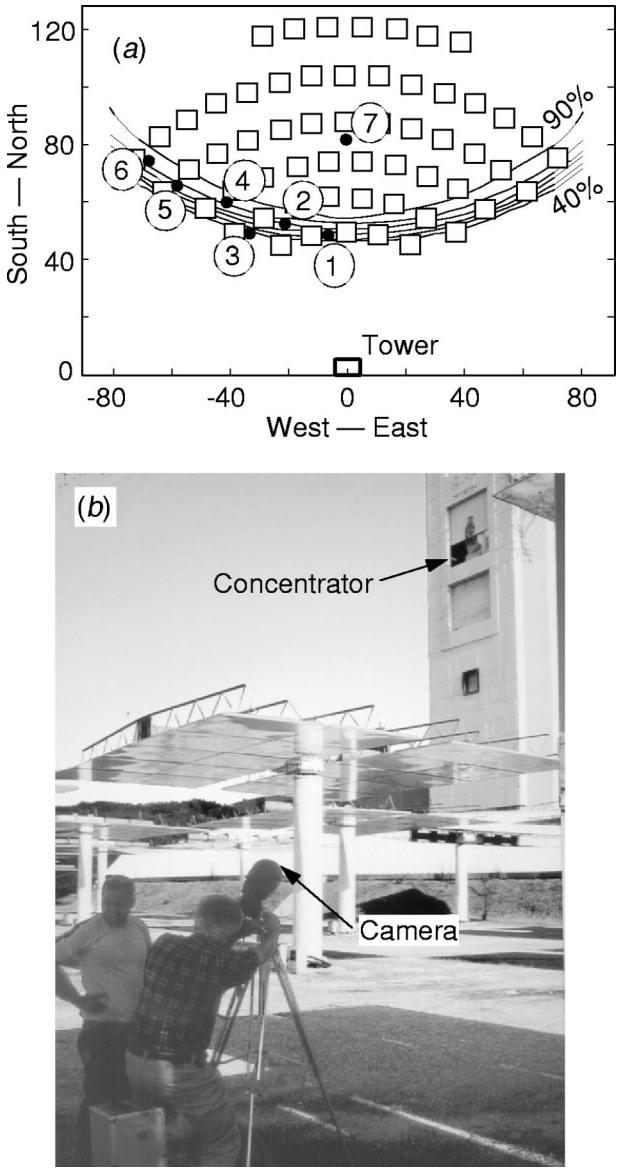

Fig. 2 (*a*) The layout of the Weizmann Institute heliostat field. The positions of the heliostats are marked as squares. The lines are equal transmission contours as predicted by ray-tracing simulations. The positions of observation for the measurement are shown as numbered dots. (*b*) The measurement system.

The scanned images were processed to exclude the rejection regions, seen as reflected ambient light, from the patterns. The goal was to reach the same contrast between the transmission and rejection zones as was achieved in the laboratory measurements, where ambient light was suppressed [14]. The pictures were separated into the three RGB color channels. A new image was produced with the following rules: a pixel containing a large red component but no significant blue component is considered to originate at the orange source and corresponds to a transmission area. A pixel containing a significant blue and not much red is considered to originate in the environment and corresponds to a rejection area. This choice obviously depends on the specific color chosen for the source at the concentrator exit aperture; a pure primary color (corresponding to one of RGB channels) would simplify the contrast criterion. The result of the filtering process is a high-contrast gray-level image with the orange features highlighted, and the ambient light suppressed. Figure 4 shows the processed transmission patterns corresponding to positions 1–6 in the field. A comparison of image 1 in Fig. 4 to Fig. 3 demonstrates the effectiveness of this procedure in eliminating ambient light.

4.2 Simulated Images. A model of the concentrator geometry was constructed for the simulation, including several free parameters that may vary to represent manufacturing and assembly errors. Eight linear dimensions which define the concentrator geometry and the slope angle (down from horizontal) were used. The next section presents the sensitivity of the simulation results to two of these parameters, one of the linear dimensions and the slope angle. The ray-tracing simulation was performed using the commercial optics code ASAP (Breault Research Organization, Tucson, AZ). The distribution of rays was organized according to the resolution of the scanned image, such that a single ray was traced for each pixel in the image. The tracing started from the concentrator's inlet aperture and proceeded towards the exit aperture. A ray was marked as transmitted if it reached the exit aperture, and rejected if it was turned around and reached the inlet aperture. About 45,000 rays were traced for each image, requiring about one minute of processing time on a PC.

Figure 5*a* shows a simulated pattern for position 1, corresponding to the measured pattern 1 in Fig. 4. One ray was traced in the simulation for each pixel in the measured pattern. The different gray levels within the transmission regions correspond to attenuation due to a different number of reflections. The brightest band in the lower right edge of the aperture corresponds to direct sight of the exit aperture from the position of observation, i.e., direct transmission of light without reflection.

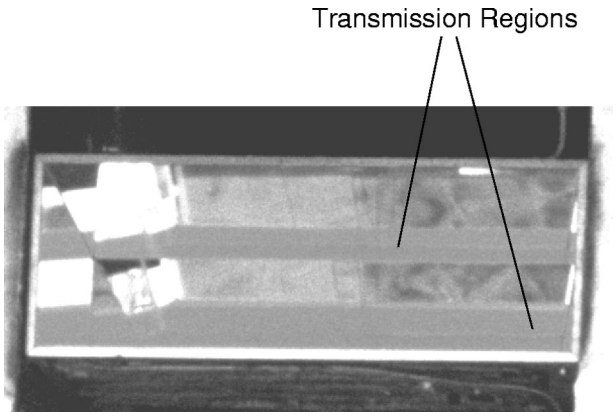

Fig. 3 Transmission pattern photograph corresponding to position 1. Transmission regions are the two relatively uniform horizontal gray strips (bright orange in the original color photograph).

4.3 Pattern Matching and Concentrator Geometry. Information about the actual geometry of the concentrator as manufactured and assembled was obtained by matching the measured transmission patterns to simulated patterns, using the following procedure. The simulated pattern and the measured pattern were overlaid and compared pixel-by-pixel. Figure 5*b* shows the difference between the two patterns. Matching areas, i.e., showing transmission in both the simulation and in the measurement, or rejection in both the simulation the measurement, are shown as white. Two types of mismatch are shown as gray areas. Pixels that appear bright in the measurement but not in the simulation are shown in light gray. Pixels that appear bright in the simulation but not in the measurement are shown in dark gray. The sum of these two types of mismatch is the total mismatch. The amount of mismatch is found by simple pixel counting in the difference image. The significant mismatch (of both types) between the patterns indicates that the actual concentrator geometry is different from the design geometry, due to errors in the manufacturing or the assembly and alignment of the concentrator.

The accuracy of the mismatch values depends on image quality and resolution. The measured image should be sharp, such that the transition between the transmission and rejection regions occurs over a single pixel. The experimental uncertainty in the area of each region is therefore proportional to the number of pixels on the boundaries of the region, since the exact transition line could be anywhere between the center of one pixel and the center of its neighbor on the other side of the boundary. The assumption that the transition is exactly between the neighbor pixels has then a maximum error of half a pixel size, and an average error value can be set as a quarter of a pixel. The same argument applies to the simulated image where again each finite pixel area is represented by a single ray located at its center. The actual tracing of the ray is exact (up to the computer round-off) and therefore contributes no additional error. For a typical case in our analysis, an image has two mismatch regions in the form of elongated strips, having four boundaries, each about 370 pixels long. The error in mismatch area, relative to the aperture area, contributed by each boundary is $370/4/45{,}000 = 0.002$. Combining the four contributions as a sum-of-squares (since statistically the errors do not have to be in the same direction), the total error estimate is 0.004 or 0.4% of the aperture area.

The geometric transmission of the concentrator for radiation incident from the observation point is defined as the ratio of the transmission area to total aperture area in the image. This is distinct from the radiation transmission, since the losses due to imperfect reflectivity are not taken into account. The geometric transmission is not necessarily very different between measurement and simulation, even when the mismatch is large. The difference in geometric transmission equals the difference between the two types of mismatch. In the example of Fig. 5*b*, the mismatch areas of the two types is nearly equal, and therefore the total difference in geometric transmission between measurement and simulation is small for this observation point (not necessarily for other observation points). This demonstrates the detailed information content of the transmission pattern measurement, which is lost when using integral measurement methods such as calorimetry.

The next step is adjustment of the geometric model of the concentrator in the simulation and seeking a better match between measurement and simulation. The procedure used was a manual adjustment of the geometric parameters, one at a time, and observing the effect of each change on the mismatch. The possibility of

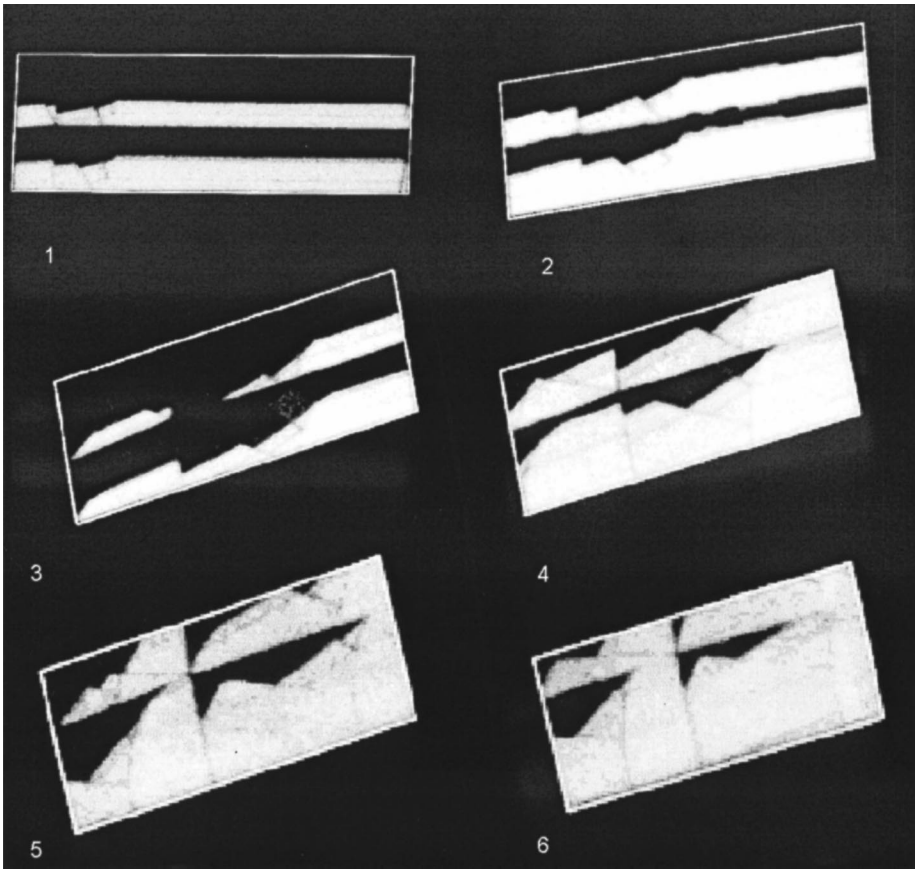

Fig. 4 Photographs of the transmission patterns after pre-processing. Numbers indicate the positions of observation. The different resolution of the photographs is due to the different camera distance to the concentrator for the different positions within the field.

automating this process, and issues that may arise in more complex models of large concentrators, are discussed in Section 5. While each parameter was changed, the mismatch in all observation points was examined. The matching of specific topological features in the transmission pattern, as well as the amount of mismatch area, were used as criteria for improvement. We have found that in general an improvement occurred simultaneously in all parts of the image, and in all the images from the different observation points.

Physical measurement of the concentrator facets before assembly has shown that the length of the front axial section (L_1 in Fig. 1) was higher than the design by three millimeters. The second axial section was shorter by the same amount, such that the total length L was correct. To see if this error can be detected, the dimension L_1 was varied in the simulation according to the procedure outlined above, and the best match was found at the correct length. Figure 6*a* shows the pixel mismatch for observation position 1 when L_1 is varied in the simulation. The correct length can be easily identified as having the lowest total mismatch. This geometric information cannot be derived from a calorimetric measurement, because the total transmission is not sufficiently sensitive to this error, as seen in Fig. 6*a*. The sensitivity of the pattern matching method, on the other hand, easily identifies errors of 1 millimeter magnitude or even smaller. A similar optimal match at the same value of L_1 was observed in the images of the other observation points.

A different type of geometric parameter value that can be easily detected is the alignment of the concentrator. Figure 6*b* shows the pixel mismatch while varying the tilt angle of the concentrator axis downward from horizontal in the simulation. In this case the minimum in the total mismatch curve is less pronounced. However, the optimal value is easy to identify since it provides the best balance between the two types of mismatch. In this case, the total transmission shows reasonable sensitivity to the slope parameter, indicating that a calorimetric measurement could in principle be used to detect the correct concentrator slope. However, experimental errors in a calorimetric measurement make it very difficult to obtain the measurement accuracy of about 1% that is needed here. The transmission patterns can be measured with negligible error, since high image resolution is easy to achieve. It is, therefore, possible to detect concentrator slope errors as small as 0.1° or even smaller.

Figure 7 shows the effect of the optimization of the length parameter L_1 on the mismatch at all positions of observation. The slope angle parameter was already corrected in these results. The reduction in mismatch is significant, indicating that the concentrator geometry in the simulation model is very close to the actual geometry. The remaining total mismatch of about 5% is due to the other geometric parameters that were not varied within this analysis.

5 Discussion

We have demonstrated an *in-situ* application of the remote optical assessment method for nonimaging concentrators. The measurement was performed in a full-scale solar tower facility, using easily available technical equipment. The measurement did not require contact with the concentrator, except for the placement of a flat surface at the exit aperture. Analysis of the measured transmission patterns provided accurate information on the actual values of several geometric parameters of the concentrator. Compared to an integral calorimetric test of a concentrator, the remote optical method provides much more geometric information and much higher accuracy. Compared to photogrammetry, the remote optical measurement enables measurement of devices with deep geometry and a non-uniform number of reflections, and does not

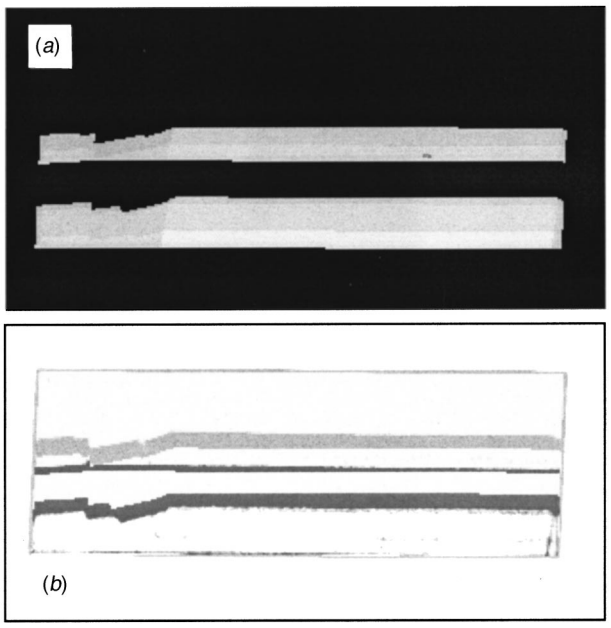

Fig. 5 (*a*) Simulated transmission pattern for the observation position 1. Gray levels correspond to different numbers of reflections. (*b*) The differences between the measured and simulated patterns; simulated geometry of the concentrator was according to the original design.

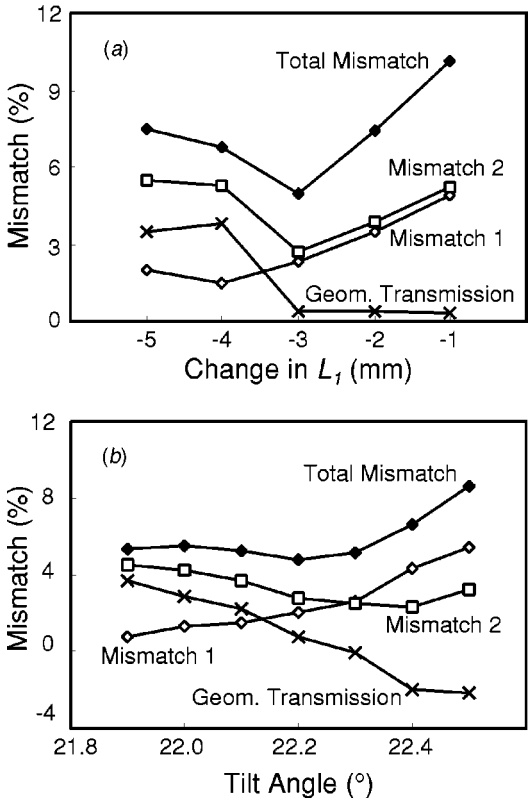

Fig. 6 Pixel mismatch and the difference in geometric transmission for observation position 1. (a) Variation of the axial position of the intermediate aperture in the geometry used for the simulation; (b) Variation of tilt angle of the concentrator axis downward from horizontal. Mismatch 1: pixels when the simulation is bright but the measurement is not. Mismatch 2: pixels where the measurement is bright but the simulation is not.

require contact with or manipulation of the reflective surfaces. Our method for non-imaging secondary concentrators can complement photogrammetry used for primary concentrators, to provide a complete solution for characterization of two-stage optical systems.

The high sensitivity of the pattern matching procedure provided high-resolution values of the concentrator geometric parameters that were varied in our analysis. Variations of 1 mm in linear dimension and 0.1° in tilt angle were detected. The accuracy of the measurement depends on the resolution of the measured and simulated images. The resolution of the measurement is mainly limited by distortions induced by the optical equipment and by the air. In our tests, these effects were not significant and did not limit the measurement accuracy. The resolution of the simulated results can be chosen as desired, with higher resolution resulting in somewhat higher (but not excessive) computational effort.

Small-scale geometric imperfections in the mirrors can influence the measured images, but these effects were found insignificant in our tests. The boundaries between areas of different color in the images were quite sharp, up to image resolution, showing that any diffuse component in the reflection or small-scale waviness that creates effective scattering, were not significant. Straight edges observed through a reflection in the mirrors are seen as straight lines, with hardly any distortion. This indicates that long-wave deformation of the mirrors is also insignificant up to the limit of image resolution. We expect that specularity will not be an issue in most well manufactured concentrators. Long-wave deformations may exist, especially in large facets, and should be identified and corrected. This can be done by modeling each facet with additional degrees of freedom for curvature, and calibrating the additional parameters using the distortions found in the measured transmission patterns.

The question of uniqueness and local minima is always present in optimization problems. The rudimentary test presented here of matching two geometric parameters to known values was successful, but this is no guarantee for success in general. We believe that for this particular application, the danger of misleading local minima is not severe. First, the initial guess should be close to the desired solution, since the geometric deviations sought should be relatively small for a reasonable concentrator. Second, the amount of information to be matched is large and complex. In principle, each pixel in an image can be regarded as a bit of information, leading to 45,000 bits to be matched per image in our tests. Some of this information represents a complex interaction of many parameters via multiple reflections. It is unlikely that different combinations of geometric parameters will reproduce the same complex set of information embodied in the transmission patterns from different observation points. We have no rigorous proof of this conjecture; the best way to gain confidence in this issue is probably by accumulating experience in using this procedure with different cocentrators.

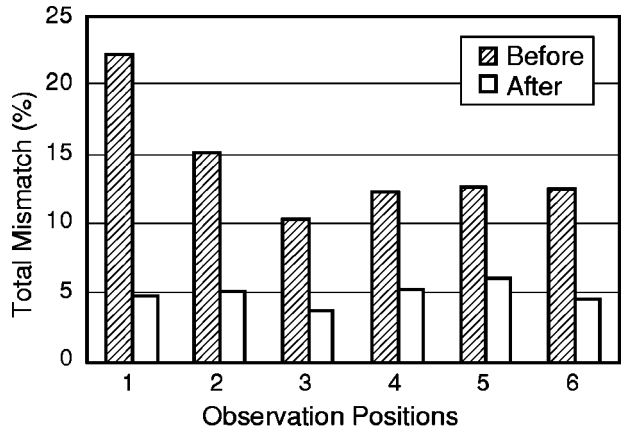

Fig. 7 Total pixel mismatch before and after the optimization of the position for the intermediate aperture L_1. The tilt angle of the concentrator axis has already been optimized.

In addition to the geometric model of the concentrator, the optimization may benefit from a few other free parameters. The orientation angles of the concentrator's axis can be accurately found from optimization of the pattern match, as shown above. Other parameters that were not varied in the current work are the concentrator's position in the tower and the positions of the observation points in the field. The selection of the appropriate free parameters for optimization depends on the uncertainty in the values that these parameters are assigned before the remote measurements.

In principle, the effect of different parameters in the geometric model can be coupled, so that finding an optimum by varying one parameter at a time is difficult. We have found that it is possible to decouple the parameters by a correct ordering of the 1-D parameter searches. The reason for this behavior is that some features in the transmission pattern are strongly affected by specific parameters, and less affected by others. For example, the geometry of the apertures observed in the image is affected by a global parameter such as the concentrator tilt angle, but not by other parameters that define internal structure like L_1. The tilt angle can be determined by focusing on specific features in the images. Another important effect is that radiation leaving the exit aperture always travels towards the inlet aperture, and cannot turn back. The pattern observed at the facets adjacent to the exit aperture is not affected by the geometry of facets farther towards the inlet aperture. The parameters defining the first ring of facets can then be determined separately from the rest of concentrator by matching only the part of the transmission pattern that is viewed through these facets. The same argument can be made by induction for each successive ring of facets, after the geometry of the previous ring has been determined.

In a large concentrator composed of many facets, the number of degrees of freedom in the geometric model can be large, requiring a higher computational load in the matching process. The decoupling process described above can alleviate the computational load, but it would still be a challenge. Therefore, it is desirable to construct a geometric model of the concentrator that is simplified as much as possible. The simplification should be based on analysis of the concentrator construction method and identification of the main types of geometric errors that would be expected.

The number of required observation points needed to fully characterize a concentrator should be related to the number of degrees of freedom in the concentrator's geometric model. A practical procedure for a large and complex concentrator can be as follows. Analyze a small number of patterns, say from three observation points. Optimize the geometric model based on these patterns. Then measure a few additional patterns from different positions, and test whether the optimized model provides a good match to these patterns as well. If not, re-optimize with the larger set of patterns. Then repeat the test with new patterns. This incremental procedure should allow a reasonable compromise between effort and accuracy.

The analysis described here can be partly automated, but manual intervention and control for the high-level decisions are recommended. For a given type of concentrator, some expertise will be needed in order to define the decoupling and optimization order of the parameters in the model, and to identify which features in the pattern should be matched for specific parameters. This is important when the method is applied for a complex concentrator with a large number of degrees of freedom and of observation points, since the amount of computation for a fully automatic optimization could be prohibitive.

Application of the remote measurement to solar plants which are much larger than the WIS field should be similar to the current application. As the heliostat field increases in size, the concentrator inlet aperture will also increase by roughly the same ratio. The

required optical setup is therefore similar, and possibly the only effect will be somewhat higher interference due to the intervening air between the camera and the target.

Acknowledgment

This work was supported by the Israeli Ministry of Science (MOS) under the aegis of KFA-BEO-Forschungszentrum Jülich GmbH/Projektträger für Biologie, Energie und Ökologie, and by the German Federal Ministry of Economy (BMWi). We thank C. Barak of the Weizmann Institute photography department for taking the high quality photographs.

References

[1] Welford, W. T., and Winston, R., 1989, *High Collection Non-Imaging Optics*, Academic Press.
[2] Friedman, R. P., Gordon, J. M., and Ries, H., 1996, ''Compact High-Flux Two-Stage Solar Collectors Based on Tailored Edge-Ray Concentrators,'' Sol. Energy, **56**, pp. 607–615.
[3] O'Gallagher, J., and Winston, R., 1986, ''Test of a Trumpet Secondary Concentrator with a Paraboloidal Dish Primary,'' Sol. Energy, **36**, pp. 37–44.
[4] Levy, I., and Epstein, M., 1998, ''Design and Operation of a High-Power Secondary Concentrator,'' 9th *Int. Symp. on Solar Thermal Concentrating Technologies*, G. Flamant, A. Ferriere, and F. Pharabod (eds.), Odeillo, EDP Sciences, pp. 575–580.
[5] Buck, R., Abele, M., Kunberger, T., Denk, T., Heller, P., and Lüpfert, E., 1998, ''Receiver for Solar-Hybrid Gas Turbine and Combined Cycle Systems,'' 9th *Int. Symp. on Solar Thermal Concentrating Technologies, Journal de Physique IV*, G. Flamant, A. Ferriere, and F. Pharabod (eds.), Odeillo, EDP Sciences, 9, pp. 537–544.
[6] Gordon, J. M., and Ries, H., 1993, ''Tailored Edge-Ray Concentrators as Ideal Second Stage for Fresnel Reflectors,'' Appl. Opt., **32**, pp. 2243–2251.
[7] Kribus, A., Zaibel, Z., Segal, A., Carey, D., and Karni, J., 1998, ''A Solar-Driven Combined Cycle Plant,'' Sol. Energy, **62**, pp. 121–129.
[8] Yogev, A., Kribus, A., Epstein, M., and Kogan, A., 1998, ''Solar 'Tower Reflector' Systems: A new Approach for High-Temperature Solar Plants,'' Int. J. Hydrogen Energy, **23**, pp. 239–245.
[9] Fletcher, E. A., and Moen, R. L., 1977, ''Hydrogen and Oxygen from Water,'' Science, **197**, p. 1050.
[10] Steinfeld, A., Kuhn, P., and Reller, A., 1998, ''Solar-Processed Metals as Clean Energy Carriers and Water-Splitters,'' Int. J. Hydrogen Energy, **23**, pp. 767–774.
[11] Kribus, A., Huleihil, M., Timinger, A., and Ben-Mair, R., 2000, ''Performance of a Rectangular Secondary Concentrator with an Asymmetric Heliostat Field,'' Sol. Energy, **69**, pp. 139–151.
[12] Suresh, D., O'Gallagher, J., and Winston, R., 1990, ''Thermal and Optical Performance Test Results for Compound Parabolic Concentrators (CPCs),'' Sol. Energy, **44**, pp. 257–270.
[13] Shortis, M., and Johnston, G., 1997, ''Photogrammetry: An Available Surface Characterization Tool for Solar Concentrators, Part II: Assessment of Surfaces,'' ASME J. Sol. Energy Eng., **119**, pp. 286–291.
[14] Timinger, A., Kribus, A., Ries, H., Smith, T., and Walther, M., 2000, ''Optical Assessment of Nonimaging Concentrators,'' Appl. Opt., **39**, pp. 5679–5684.
[15] Timinger, A., Spirkl, W., Kribus, A., and Ries, H., 2000, ''Optimized Secondary Concentrators for a Partitioned Central Receiver System,'' Sol. Energy, **69**, pp. 153–162.
[16] Doron, P., and Kribus, A., 1996, ''Receiver Partitioning: A Performance Boost for High-Temperature Solar Applications,'' 8th *Int. Symp. on Solar Thermal Concentrating Technologies*, M. Becker and M. Böhmer (eds.), C. F. Köln Müller, 2, pp. 621–630.
[17] Kribus, A., Doron, P., Karni, J., Rubin, R., Reuven, R., Taragan, E., and Duchan, S., 2000, ''A Multistage Solar Receiver: The Route to High Temperature,'' Sol. Energy, **67**, pp. 3–11.